Article

Neutron Diffraction and Computer Simulation Studies of d-Xylose

Philip E. Mason, George W. Neilson, John E. Enderby, Marie-Louise Saboungi, and John W. Brady

J. Am. Chem. Soc., **2005**, 127 (31), 10991-10998• DOI: 10.1021/ja051376l • Publication Date (Web): 15 July 2005

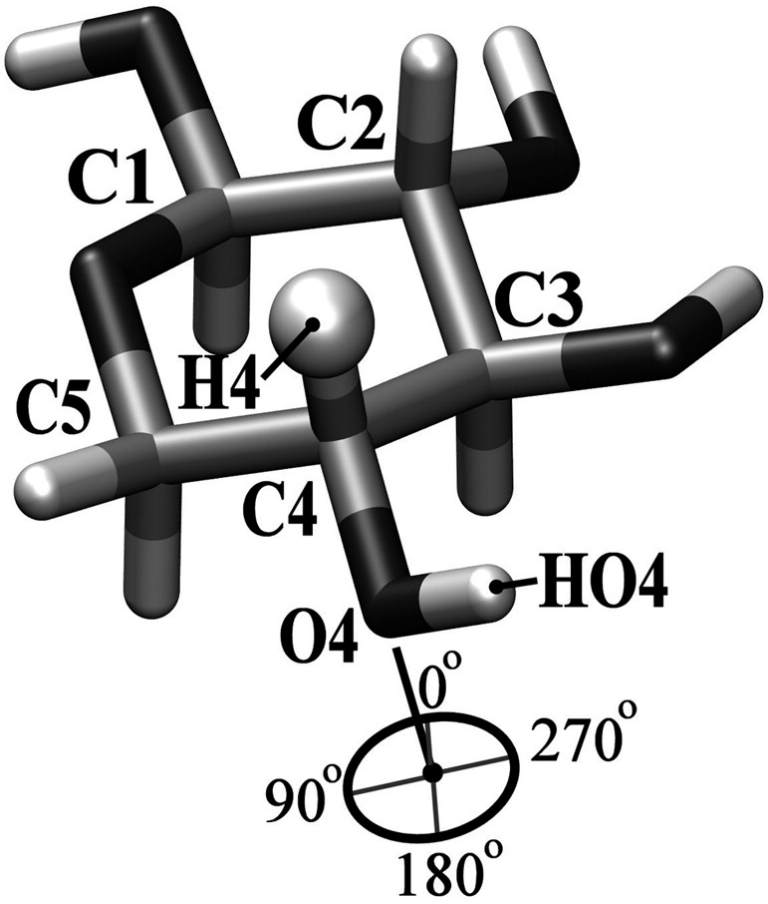

More About This Article

Additional resources and features associated with this article are available within the HTML version:

- Supporting Information
- Links to the 2 articles that cite this article, as of the time of this article download
- Access to high resolution figures

J|A|C|S
ARTICLES
Published on Web 07/15/2005

Neutron Diffraction and Computer Simulation Studies of D-Xylose

Philip E. Mason,[†] George W. Neilson,[‡] John E. Enderby,[‡]
Marie-Louise Saboungi,[#] and John W. Brady*,[†]

Contribution from the Department of Food Science, Stocking Hall, Cornell University, Ithaca, New York 14853, H.H.Wills Physics Laboratory, University of Bristol, Bristol BS8 1TL, U.K., and Centre de Recherche sur la Matière Divisée, 1 bis rue de la Férollerie, 45071 Orléans, France

Received March 4, 2005; E-mail: jwb7@cornell.edu

Abstract: Neutron diffraction with isotopic substitution (NDIS) experiments and molecular dynamics (MD) simulations have been used to examine the pentose D-xylose in aqueous solution. By specifically labeling D-xylose molecules with a deuterium atom at the nonexchangeable hydrogen position on C4, it was possible to extract information about the atomic structuring around just that specific position. The MD simulations were found to give satisfactory agreement with the experimental NDIS results and could be used to help interpret the scattering data in terms of the solvent structuring as well as the intramolecular hydroxyl conformations. Although the experiment is challenging and on the limit of modern instrumentation, it is possible by careful analysis, in conjunction with MD studies, to show that the conformation trans to H4 at 180° is strongly disfavored, in excellent agreement with the MD results. This is the first attempt to use NDIS experiments to determine the rotameric conformation of a hydroxyl group.

Introduction

The way in which solutes interact with water in aqueous solutions has important consequences for the properties of the solutions. These interactions, for example, are responsible for the folding of globular proteins and the organization of lipids into bilayers and micelles, and underlie the mechanism of the Hofmeister series for ions. As these examples suggest, the interactions of a particular solute with water are a specific and complex function of the molecular topology of the solute.[1] On the basis of measurements of macroscopic properties such as the entropy, solutes have long been characterized broadly as "structure makers" and "structure breakers".[2,3] However, the actual experimental characterization of solvent structuring at the molecular level has proven to be difficult. Molecular mechanics simulations have been able to provide detailed pictures of how complex biological solutes interact with water and how this solvent structuring is a sensitive function of the solute molecular topology,[1,4−6] but thus far it has not been possible to verify directly these predictions using experimental data. On the other hand, neutron diffraction is a powerful experimental technique for probing in detail the structure of such aqueous solutions, but interpretation of the results for complex chiral molecules remains a challenge.

Because of these difficulties, previous work on aqueous solutions has focused mainly on simple electrolytes, although the solvent structuring induced by chiral molecular solutes such as peptides or sugars is of greater biological interest.[1,6] Probing solvent structuring for complex solutes with neutron diffraction has been hampered by the fact that the measured total structure factor contains atomic correlations from each of the atom pairs in the solution. Neutron diffraction with isotopic substitution (NDIS) experiments reduce this complexity by exploiting the difference in coherent neutron scattering cross sections between different isotopes of the same element. By taking the difference between the measured scattering in two chemically identical samples, in one of which an element is completely replaced by an isotope with a sufficiently different scattering cross section, all scattering contributions not involving this atom will cancel out. Since the isotopes of oxygen and carbon have insufficient contrast in their coherent neutron scattering lengths for such experiments, even using state-of-the-art neutron facilities, the substitution of hydrogen with deuterium offers the only currently practical opportunity to use the NDIS technique to study sugars in water.

A significant number of the reported NDIS studies of molecular solutes have been for glucose[7−9] due to its high

[†] Cornell University.
[‡] University of Bristol.
[#] Centre de Recherche sur la Matière Divisée.

(1) Liu, Q.; Brady, J. W. *J. Am. Chem. Soc.* **1996**, *118*, 12276−12286.
(2) Franks, F. In *Water: A Comprehensive Treatise*; Franks, F., Ed.; Plenum Press: New York, 1973; Vol. 2, pp 1−54.
(3) Ohtaki, H.; Radnai, T. *Chem. Rev.* **1993**, *93*, 1157−1204.
(4) Ha, S.; Gao, J.; Tidor, B.; Brady, J. W.; Karplus, M. *J. Am. Chem. Soc.* **1991**, *113*, 1553−1557.
(5) Brady, J. W. *Forefronts/Cornell Theory Center* **1993**, *9*, 7.
(6) Schmidt, R. K.; Karplus, M.; Brady, J. W. *J. Am. Chem. Soc.* **1996**, *118*, 541−546.
(7) Sidhu, K. S.; Goodfellow, J. M.; Turner, J. Z. *J. Chem. Phys.* **1999**, *110*, 7943−7950.
(8) Mason, P. E.; Neilson, G. W.; Barnes, A. C.; Enderby, J. E.; Brady, J. W.; Saboungi, M.-L. *J. Chem. Phys.* **2003**, *119*, 3347−3353.
(9) Mason, P. E.; Neilson, G. W.; Enderby, J. E.; Saboungi, M.-L.; Brady, J. W. *J. Phys. Chem. B* **2005**, *109*, 13104−13111.

10.1021/ja051376l CCC: $30.25

solubility in water and archetypal character. As the most abundant and prototypical sugar, D-glucose is arguably the most biologically important carbohydrate. Understanding the roles of carbohydrates in biological systems requires a knowledge of the behavior of glucose in a range of situations, concentrations, temperatures, etc. As might therefore be expected, glucose has been the subject of more experimental and theoretical investigations than any other sugar.[8,10−18] However, for the purpose of studying solvent structuring by sugars, glucose is perhaps not the optimal model. The exocyclic hydroxymethyl group in hexapyranoses introduces an additional degree of freedom, the ability to rotate about the C5−C6 bond, complicating the solvent structuring pattern, since each of the three principal rotamers for this group will produce a different solvent structuring. In addition, the energetics of the other hydroxyl groups, as well as the anomeric equilibrium, will be affected to some extent by the orientation of this group. It follows that a better choice for studies of the hydration of glucose-like sugars is D-xylose, the pentose analogue of D-glucose. Like glucose, xylose exists primarily in the $^4C_1$ conformation of the pyranose ring form in aqueous solution, as determined by NMR,[19] and has virtually the same 64% β:36% α anomeric ratio as glucose.[20] It is also a better subject for quantum mechanical ab initio studies since it contains two fewer heavy atoms and four fewer atoms overall, as well as having only 81 combinations of low-energy hydroxyl rotameric states, as opposed to 729 important low-energy rotameric states for glucose. Because of these advantages, the conformational and solution properties of xylose have also been the subject of both computational and experimental studies.[6,21−24] Here we report results obtained from a combination of NDIS experiments and molecular dynamics (MD) simulations to examine the solvation and conformations of D-xylose in aqueous solution.

The complexity of sugar solutes presents difficulties even in an NDIS experiment, since each of the hydrogen atoms in the chiral sugars is in a distinct environment. In this context, it should be remembered that the hydrogen atoms in sugar molecules divide into two distinct populations: readily exchangeable protons H_{ex} bound to the hydroxyl oxygen atoms, and nonexchangeable aliphatic hydrogen atoms H_{non} bound to the carbon atoms (see Figure 1). Even in a typical NDIS experiment on a pentose sugar such as D-xylose in which the nonexchangeable hydrogen atoms have been fully deuterated, the observed scattering will reflect an average over the scattering from all six nonexchangeable protons. However, the local anisotropic solvent structuring relative to each of these nonexchangeable hydrogen atoms is potentially different. Significant information could be gained from NDIS experiments if the difference scattering were due to a single substitution in a specific location of the molecule. A sugar specifically labeled with a hydrogen/deuterium substitution at one particular location could then be used in an appropriately designed NDIS experiment, paired with the natural-abundance molecule, to produce the radial distribution function for just that one atom in its asymmetric environment, thus providing an experimental probe of local solvent structuring and a test of the reliability of the results of MD simulations and the force fields used in these calculations.

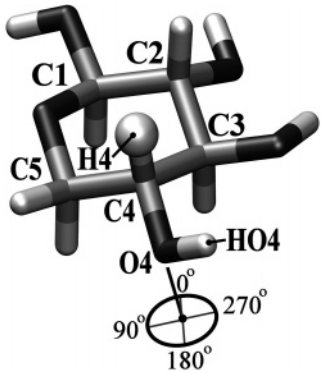

Figure 1. Schematic illustration of the β-D-xylopyranose molecule. The substituted nonexchangeable hydrogen atom on C4 is highlighted as a white ball. An indication of how the torsional angle about the C4−O4 bond is defined is included.

The studies reported here were designed to accomplish just such a comparison between simulations and the experimental scattering for a singly labeled sugar molecule. NDIS experiments were conducted for D-xylose specifically labeled at the C4 carbon by a substitution of the aliphatic hydrogen bound to this carbon atom with a deuterium atom (see Figure 1). The neutron scattering was measured for both the labeled and natural abundance xylose samples in both H_2O and D_2O solutions. The measured structure for this H4 atom was then compared to the results of MD simulations of the same system. It should be noted that, in addition to probing the solvent structure, the measured difference function contains information about the rotameric conformation of the exchangeable hydrogen of the O4 hydroxyl group. Since the intrinsic trigonometric torsional potential energy function for this hydrogen has three stable positions corresponding to the three principal staggered rotamers for that group,[25,26] with the two positions gauche to H4 having a different H4−OH4 distance from the trans position, the NDIS results allow the extraction of information about the relative populations of these states, and thus about the conformations of that hydroxyl group. Since there is presently no other way to obtain directly such information, these results become particularly useful in further evaluating the physical reliability of the intramolecular

(10) Brown, G. M.; Levy, H. A. *Science* **1965**, *147*, 1038−1039.
(11) Christofides, J. C.; Davies, D. B. *J. Chem. Soc., Perkin Trans. II* **1987**, *1987*, 97−102.
(12) Brady, J. W. *J. Am. Chem. Soc.* **1989**, *111*, 5155−5165.
(13) Barrows, S. E.; Dulles, F. J.; Cramer, C. J.; French, A. D.; Truhlar, D. G. *Carbohydr. Res.* **1995**, *276*, 219−251.
(14) Barrows, S. E.; Storer, J. W.; Cramer, C. J.; French, A. D.; Truhlar, D. G. *J. Comput. Chem.* **1998**, *19*, 1111−1129.
(15) Cramer, C. J.; Truhlar, D. G. *J. Am. Chem. Soc.* **1993**, *115*, 5745−5753.
(16) Glennon, T. M.; Merz, K. M. *J. Mol. Struct. (THEOCHEM)* **1997**, *395*, 157−171.
(17) Csonka, G. I.; Éliás, K.; Csizmadia, I. G. *Chem. Phys. Lett.* **1996**, *257*, 49−60.
(18) Dauchez, M.; Derreumaux, P.; Vergoten, G. *J. Comput. Chem.* **1992**, *14*, 263−277.
(19) Shallenberger, R. S. *Advanced Sugar Chemistry: Principles of Sugar Stereochemistry*; AVI Publishing Co., Inc.: Westport, CT, 1982.
(20) Kabayama, M. A.; Patterson, D.; Piche, L. *Can. J. Chem.* **1958**, *36*, 557−562.
(21) Jeffrey, G. A.; Robbins, A.; McMullan, R. K.; Takagi, S. *Acta Crystallogr.* **1980**, *B36*.
(22) Höög, C.; Widmalm, G. *J. Phys. Chem. B* **2001**, *105*, 6375−6379.
(23) Hricovini, M.; Malkina, O. L.; Bizik, F.; Nagy, L. T.; Malkin, V. G. *J. Phys. Chem. A* **1997**, *101*, 9756−9762.
(24) Behrends, R.; Cowman, M. K.; Eggers, F.; Eyring, E. M.; Kaatze, U.; Majewski, J.; Petrucci, S.; Richman, K.-H.; Reich, M. *J. Am. Chem. Soc.* **1997**, *119*, 2182−2186.
(25) Ha, S. N.; Giammona, A.; Field, M.; Brady, J. W. *Carbohydr. Res.* **1988**, *180*, 207−221.
(26) Palma, R.; Zuccato, P.; Himmel, M. E.; Liang, G.; Brady, J. W. In *Glycosyl Hydrolases in Biomass Conversion*; Himmel, M. E., Ed.; American Chemical Society: Washington, DC, 2000; pp 112−130.

force field. The results reported here represent the first attempt to use NDIS techniques to determine hydroxyl conformations.

Methods

Experimental Procedures. All neutron diffraction data were collected at the Institut Laue-Langevin in Grenoble under ambient conditions on the D20 diffractometer, which has a Q-range from 0.9 to 13.0 Å^{-1}. The samples were run in a cylindrical-geometry can with 0.5 mm null scattering titanium−zirconium walls and a sample diameter of 6 mm. The wavelength used was 0.7 Å, with data being collected over the angular range of 6°−139°. The multiple scattering and absorption corrections were carefully performed using literature procedures that take account of the background and sample container scattering.[27,28]

A sample of 98% enriched D4-labeled D-xylose was purchased from Omicron, while natural abundance D-xylose was obtained from Sigma (Sigma ultrapure). The same sugar samples were used for preparing both the H_2O and D_2O solutions. The method used for preparing both sugar solutions was as follows. To an accurately measured amount of xylose, the appropriate amount of light water to make a 3 molal (M*) solution (ca. 2 mL) was added gravimetrically into the null-scattering Ti/Zr can. After 8 h of collection of neutron scattering data, the entire sample was quantitatively transferred to a 25 mL pear flask of known mass, using D_2O washings, and the solvent was removed on a rotary evaporator using a Teflon-headed pump on a water bath at ca. 60 °C. After the water evaporation had ceased, the flask was removed and weighed to assess the fraction of water that had been removed (typically >95%). A further 4 mL of D_2O was then added and the process was repeated. In total this process was conducted six times, after which the correct amount of D_2O was added gravimetrically to the room-temperature flask. Four hours of collection of neutron scattering data was needed for the D_2O sample to obtain better statistics than with the H_2O sample. This procedure was carried out for both the natural and isotopically labeled xylose.

Data Analysis. The first-order difference method is well documented in the literature[29−31] and relies on the assumption that solutions of identical chemical constitution, but with different isotopic concentrations of a probe nucleus, are structurally equivalent around the probe nucleus. Here we apply the first-order difference method to, first, d_4-xylose in D_2O and natural xylose in D_2O, and second, d_4-xylose in H_2O and natural xylose in H_2O solution. In all cases the ratio of xylose to water was 3:55.55, referred to hereafter as 3 M*. [This terminology M* is used instead of the conventional "molal" since molality is measured relative to 1 kg of solvent, but the same number of H_2O and D_2O molecules have different weights, making standard molality less useful in the present context.] These first-order difference experiments yield the difference functions $\Delta^{X}_{H_{sub}}(Q)$ for the structure factors,

$$^{D_2O}\Delta^{X}_{H_{sub}}(Q) = 1.21S_{H_{sub}C}(Q) + 4.98S_{H_{sub}O}(Q) - 0.68S_{H_{sub}H_{non}}(Q) + 10.04S_{H_{sub}H_{ex}}(Q) \quad (1)$$

$$^{H_2O}\Delta^{X}_{H_{sub}}(Q) = 1.21S_{H_{sub}C}(Q) + 4.98S_{H_{sub}O}(Q) - 0.68S_{H_{sub}H_{non}}(Q) - 5.54S_{H_{sub}H_{ex}}(Q) \quad (2)$$

where $S_{H_{sub}C}(Q)$ is the structure factor for carbon atoms relative to the nonexchangeable substitution-labeled hydrogen atom H_{sub}, $S_{H_{sub}O}(Q)$ is the structure factor for oxygen atoms relative to the label, $S_{H_{sub}H_{non}}(Q)$ is the structure factor for nonexchangeable protons H_{non} relative to the label, and $S_{H_{sub}H_{ex}}(Q)$ is the structure factor for all of the exchangeable hydrogen atoms H_{ex} (i.e., the hydrogen atoms of water and the hydrogen atoms on the sugar hydroxyl groups) relative to the label.[29−31] Although the counting time for the H_2O solutions (ca. 8 h) was approximately twice that for the D_2O solutions (ca. 4 h), it was found that the statistical error in the function $^{H_2O}\Delta^{X}_{H_{sub}}(Q)$ was considerably larger than that for the analogous function in D_2O. An assessment of the statistical error was obtained by placing a spline through each difference function, and then subtracting this from the original data. In each case this gave a bar of noise which was free from systematic variation. The standard deviation of this noise was 1.1 mb str^{-1} atom^{-1} for the function $^{H_2O}\Delta^{X}_{H_{sub}}(Q)$ and 0.4 mb str^{-1} atom^{-1} for the function $^{D_2O}\Delta^{X}_{H_{sub}}(Q)$, with the data re-binned into 350 points (a bin size of 0.05 Å^{-1}). While better statistical errors would always be preferable, it should be remembered that, in order to halve the statistical error, the counting time needs to be increased by a factor of 4. As the majority of the statistical error in these data comes from the H_2O solutions, for which data were collected for 8 h in the present experiment, considerably longer counting times would be required just to halve the statistical error. Due to the severe limitations on the availability of neutron beam time, this is not a practical option. However, the next generation of neutron machines currently being built may be able to offer approximately an order of magnitude higher flux and the stability of detectors required to significantly enhance the accuracy of these measurements.

The directly calculated difference function ($\Delta_{sub}(Q)$) can be Fourier transformed to real space to give the total radial distribution function ($G_{sub}(r)$) which contains structural correlations of the substituted nucleus to other atoms in the system. These data are composed of a combination of radial distribution functions weighted by prefactors, which are calculated from the atomic composition of the system, and the neutron scattering lengths of those components.

$$^{D_2O}G^{X}_{H_{sub}}(r) = 1.21g_{H_{sub}C}(r) + 4.98g_{H_{sub}O}(r) - 0.68g_{H_{sub}H_{non}}(r) + 10.04g_{H_{sub}H_{ex}}(r) \quad (3)$$

$$^{H_2O}G^{X}_{H_{sub}}(r) = 1.21g_{H_{sub}C}(r) + 4.98g_{H_{sub}O}(r) - 0.68g_{H_{sub}H_{non}}(r) - 5.54g_{H_{sub}H_{ex}}(r) \quad (4)$$

Clearly, $^{D_2O}\Delta^{X}_{H_{sub}}(Q) - {}^{H_2O}\Delta^{X}_{H_{sub}}(Q)$ yields $15.58S_{H_{sub}H_{ex}}(Q)$ (the statistical noise in this function, as calculated by the method described above, was 1.2 mb str^{-1} atom^{-1}). The H_{ex} population may be further split into exchangeable hydrogen atoms on xylose ($H_{ex}X$) and those on water ($H_{ex}W$). It is found that for a 3 M* solution,

$$15.58S_{H_{sub}H_{ex}}(Q) = 14.06S_{H_{sub}H_{ex}W}(Q) + 1.52S_{H_{sub}H_{ex}X}(Q) \quad (5)$$

which can also expressed as

$$15.58g_{H_{sub}H_{ex}}(r) = 14.06g_{H_{sub}H_{ex}W}(r) + 1.52g_{H_{sub}H_{ex}X}(r) \quad (6)$$

Further, the $S_{H_{sub}H_{ex}}(Q)$ component of $^{D_2O}\Delta^{X}_{H_{sub}}(Q)$ or $^{H_2O}\Delta^{X}_{H_{sub}}(Q)$ can be subtracted to yield a new function, e.g.,

$$^{D_2O}\Delta^{Y}_{H_{sub}}(Q) = 1.21S_{H_{sub}C}(Q) + 4.98S_{H_{sub}O}(Q) - 0.68S_{H_{sub}H_{non}}(Q) \quad (7)$$

which can be Fourier transformed to yield

$$^{D_2O}G^{Y}_{H_{sub}}(r) = 1.21g_{H_{sub}C}(r) + 4.98g_{H_{sub}O}(r) - 0.68g_{H_{sub}H_{non}}(r) \quad (8)$$

where Y denotes that this is correlated to all atoms other than H_{ex}. This residual should be the same for both solutions, i.e.,

$$^{D_2O}\Delta^{Y}_{H_{sub}}(Q) = {}^{H_2O}\Delta^{Y}_{H_{sub}}(Q) \quad (9)$$

(27) Barnes, A. C.; Enderby, J. E.; Breen, J.; Leyte, J. C. *Chem. Phys. Lett.* **1987**, *142*, 405−408.
(28) Barnes, A. C.; Hamilton, M. A.; Beck, U.; Fischer, H. E. *J. Phys.: Condens. Matter* **2000**, *12*, 7311−7322.
(29) Enderby, J. E. *Chem. Soc. Rev.* **1995**, *24*, 159−168.
(30) Neilson, G. W.; Mason, P. E.; Ramos, S.; Sullivan, D. *Philos. Trans. R. Soc.* **2001**, *A359 (1785)*, 1575−1591.
(31) Squires, G. L. *Introduction to the Theory of Thermal Neutron Scattering*; Cambridge University Press: Cambridge, UK, 1978.

This comparison gives an assessment of the accuracy of the measurements. Both of these functions share some statistical noise features, as their calculation requires, in both cases, the subtraction of the same function $S_{H_{sub}H_{ex}}(Q)$.

Simulation Procedures. In the MD simulations, a periodic cubic system was created at 3 M* concentration containing a number of independent xylose molecules surrounded by explicit water molecules. The simulations employed the CSFF sugar force field,[26,32,33] with water molecules represented by the TIP3P model.[34,35] All simulations were performed as NVE ensembles using the CHARMM program,[36] with chemical bonds to hydrogen atoms kept fixed using SHAKE[37] and a time step of 1 fs. The starting coordinates were created by placing 36 randomly orientated xylose molecules (consisting of 24 β and 12 α anomers) in a 34 Å cube. The ratio of 2 β:1 α closely resembles a D-xylose solution at the anomeric equilibrium. These coordinates were superimposed on a box of 1296 water molecules, and those which were within ca. 2.5 Å of any solute heavy atom were discarded to produce the correct concentration; by design this procedure produced a 3 M* solution (36 xylose molecules and 666 TIP3P water molecules, 3.003 molal). Finally, the box length was rescaled to 29.5851 Å, which yielded the correct physical number density (0.105 atom Å^{-3}).

All van der Waals and electrostatic interactions were smoothly truncated on a group basis using switching functions from 13 to 15 Å. Initial velocities were assigned from a Boltzmann distribution (300 K), followed by 7 ps of equilibration dynamics with velocities being reassigned every 0.1 ps. The simulation was then run for 1.5 ns with no further velocity reassignment. The first 0.5 ns of this was taken as equilibration, and the remaining 1 ns was used for analysis. The final coordinates of this 1.5 ns simulation were used as the starting coordinates for three additional simulations, where the H4−C4−O4−HO4 dihedral angle was constrained to 60°, 180°, and 300° using the harmonic dihedral constraint facility of the CHARMM program, with a constraint force constant of 200 kcal mol^{-1}. In each simulation, the initial velocities were assigned from a Boltzmann distribution at 300 K followed by 5 ps of equilibration dynamics with velocities reassigned every 0.1 ps. Each simulation was then run for an additional 0.5 ns with no further velocity reassignment. These constrained simulations were used for determining which conformation of this C4−O4 hydroxyl group gave the best match between the calculated and experimental structure factors. MD structure factors were calculated as Fourier transforms of radial distribution functions averaged over the trajectory.

Results and Discussion

Figure 2a compares the experimentally measured functions ${}^{D_2O}\Delta^{Y}_{H_{sub}}(Q)$ and ${}^{H_2O}\Delta^{Y}_{H_{sub}}(Q)$ with the $\Delta^{Y}_{H_{sub}}(Q)$ calculated from the MD simulation. The MD simulation reproduces these experimental functions remarkably well. A basic assumption of the NDIS experiment is that neither the solvent structuring nor the molecular structure of the solute is significantly affected by the isotopic substitution. Given this assumption, the functions ${}^{D_2O}\Delta^{Y}_{H_{sub}}(Q)$ and ${}^{H_2O}\Delta^{Y}_{H_{sub}}(Q)$ should be the same, and their comparison gives a measure of the experimental accuracy and reproducibility.

Figure 2 also presents the total atomic radial distribution function ${}^{H_2O}G^{Y}_{H_{sub}}(r)$ resulting from the Fourier transform of ${}^{H_2O}\Delta^{Y}_{H_{sub}}(Q)$ (Figure 2b, gray line of the middle panel). The

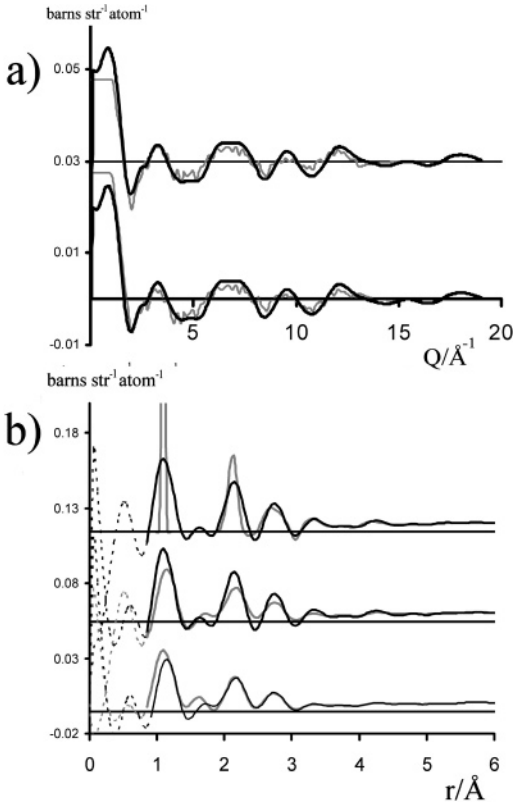

Figure 2. (a) Experimentally measured functions ${}^{H_2O}\Delta^{Y}_{H_{sub}}(Q)$ and ${}^{D_2O}\Delta^{Y}_{H_{sub}}(Q)$, gray lines, upper and lower, respectively. It is an experimental assumption that these two functions are identical. In each case the function ${}^{H_2O}\Delta^{Y}_{H_{sub}}(Q)$ predicted by MD is shown in black. (b) Upper: the function ${}^{H_2O}G^{Y}_{H_{sub}}(r)$ without experimental resolution imposed (gray) and with experimental resolution imposed (black). Middle: the experimentally measured function ${}^{H_2O}G^{Y}_{H_{sub}}(r)$ (gray) and the same function calculated from the MD simulation with the experimental resolution imposed upon it (black). Lower: comparison of the experimentally determined functions ${}^{H_2O}G^{Y}_{H_{sub}}(r)$ and ${}^{D_2O}G^{Y}_{H_{sub}}(r)$ in black and gray lines, respectively.

structure in the experimental radial distribution function at distances less than 1.0 Å arises from truncation errors and is shown as a dotted curve in this and subsequent figures. Again, there is good agreement between the MD and experimental results. In particular, the positions and relative intensities of all of the principal peaks agree closely between the experimental and MD ${}^{H_2O}G^{Y}_{H_{sub}}(r)$ values, once the experimental resolution is imposed on the simulation results. Recall that a sharp feature in *r*-space is represented in *Q*-space as a lightly damped sine wave, and that the wavelength defines the value of *r*, with shorter wavelengths representing higher *r*-space features. The damping defines the broadness of the *r*-space feature: the broader the feature, the more severe the damping. Large, broad *r*-space features are therefore severely damped, higher-frequency *Q*-space features. Molecular correlations are generally lower frequency, much less severely damped *Q*-space features. The calculated function ${}^{H_2O}\Delta^{Y}_{H_{sub}}(Q)$ exhibits significant signal above the upper experimental limit of the measurements (13 Å^{-1}) due to molecular correlations. As a result, since the experimental results are resolution limited, the sharpness of some of the correlations in the function ${}^{H_2O}G^{Y}_{H_{sub}}(r)$ is underestimated. The importance of the experimental resolution of these features can be illustrated numerically by Fourier transforming the calculated ${}^{H_2O}\Delta^{Y}_{H_{sub}}(Q)$ using the *Q*-range of the present experiments. This procedure will, in essence, impose the

(32) Kuttel, M.; Brady, J. W.; Naidoo, K. J. *J. Comput. Chem.* **2002**, *23*, 1236−1243.
(33) Kuttel, M. M. Ph.D. Thesis, University of Cape Town, Cape Town, South Africa, 2003; p 231.
(34) Jorgensen, W. L.; Chandrasekhar, J.; Madura, J. D.; Impey, R. W.; Klein, M. L. *J. Chem. Phys.* **1983**, *79*, 926−935.
(35) Neria, E.; Fischer, S.; Karplus, M. *J. Chem. Phys.* **1996**, *105*, 1902−1919.
(36) Brooks, B. R.; Bruccoleri, R. E.; Olafson, B. D.; Swaminathan, S.; Karplus, M. *J. Comput. Chem.* **1983**, *4*, 187−217.
(37) van Gunsteren, W. F.; Berendsen, H. J. C. *Mol. Phys.* **1977**, *34*, 1311−1327.

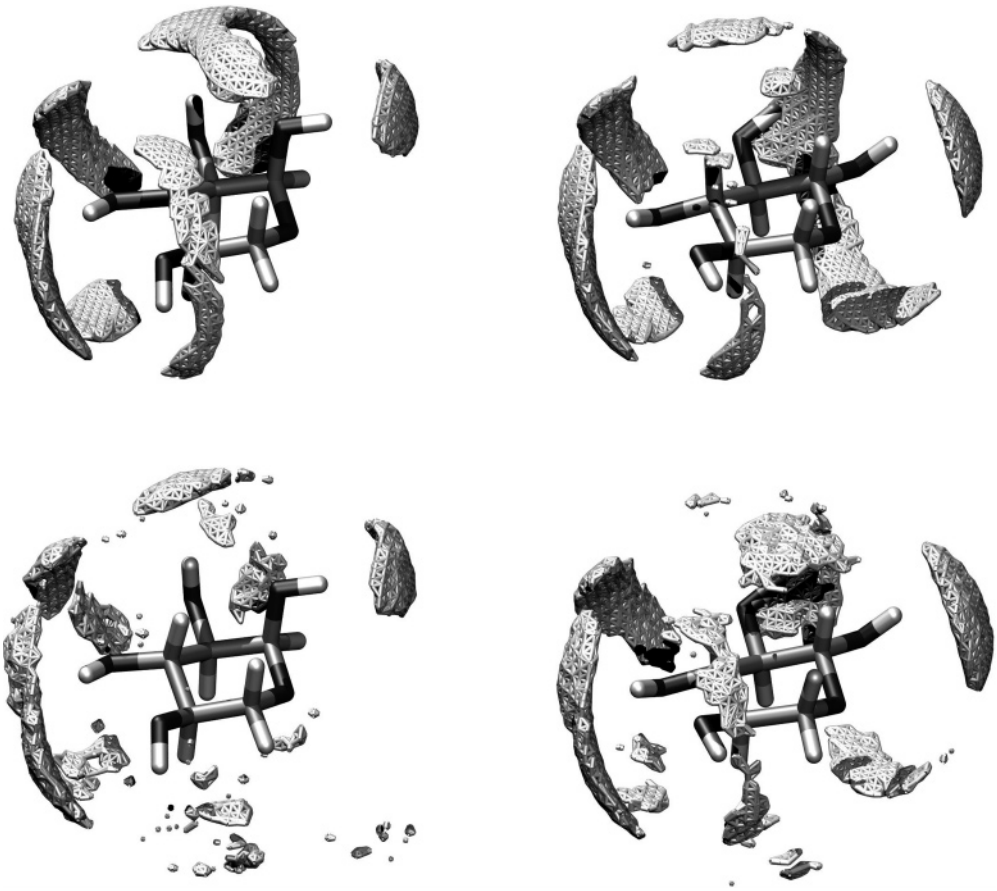

Figure 3. Contours of oxygen atom density around a reference xylopyranose molecule as calculated from the MD simulations. The top two figures show water oxygen atom density (contour level is at ND 0.02, 5.8 times the average number density of water oxygen atoms), with α-D-xylopyranose on the left (oriented such that the C4 group is in front) and β-D-xylopyranose on the right. The bottom two figures show xylose oxygen atom density around D-xylopyranose (contour level is at ND of 0.02, 2.9 times the ND of xylose oxygen atoms), with α again on the left and β on the right.

resolution limit of the experimental measurement onto the MD data (Figure 2b, top; gray line, without the experimental resolution limit; black line, with the experimental resolution). The resolution limit is most notable in the $H_{sub}C$ correlation at about 1.1 Å and, to a lesser extent, in the $\mathbf{H_{sub}}-C-\mathbf{O}$ and $\mathbf{H_{sub}}-C-\mathbf{C}$ correlations at 2.1 Å. It should be remembered that in the MD simulations all bonds to hydrogen atoms were kept fixed using the SHAKE constraint procedure.[37] While this constraint will result in the MD prediction being somewhat too sharp, previous simulations where the SHAKE procedure was not used have shown that there is little broadening of this feature when the bond is assigned a force constant. No other features in the MD data are significantly resolution-limited. The biggest differences between the MD prediction and the measured curves are in the overly sharp peaks in the MD function at 2.1 Å and 2.7 Å due to the positively weighted $\mathbf{H_{sub}}-C-\mathbf{O}$ and $\mathbf{H_{sub}}-C-\mathbf{C}$ correlations, and the negatively weighted $\mathbf{H_{sub}}-C-\mathbf{H_{non}}$ peaks at 2.5 Å and 3.1 Å. This difference can be observed in the *Q*-space data, where the NDIS function damps away faster at higher *Q* than the equivalent MD function. As similar NDIS experiments using heavy-atom substitution under comparable conditions did not exhibit such behavior,[38] it is possible that this is a consequence of quantum mechanical uncertainty in the position of the probe nucleus.

(38) Mason, P. E.; Neilson, G. W.; Dempsey, C. E.; Brady, J. W. *J. Phys. Chem. B* **2005**, submitted.

A major goal of this study was not just to probe the intramolecular structure of the solute, which in the case of sugars is relatively constrained by the rigidity of the covalent architecture, but also to determine the nature of the solvent water structuring around the solute. This can be directly calculated from the MD simulations, as has been done before,[1,4,6,7] and is displayed separately for both anomers of xylose in the upper panel of Figure 3. The solvent structuring patterns are very similar to those previously found for sugars.[1,6−9] No overall tendency for the sugar molecules to associate was observed in the MD simulations, as would be expected for xylose at this concentration. However, because of the relatively high concentration, direct interactions between sugar molecules often occurred during the course of the simulation. The lower panel of Figure 3 shows how other sugar molecules structure around a given xylose solute, and as already found for glucose,[9] these interactions are via hydrogen bonds which tend to be arranged in patterns similar to those occupied by water hydrogen bond partners. Unfortunately, the rich anisotropic detail revealed by MD simulations cannot be extracted from the experiments, which can only determine radially averaged distributions of atoms. However, such radial distribution functions can still be used to evaluate the overall validity of the simulation results.

The calculated radial distribution function $g_{H_{sub}H_{ex}}(r)$ for exchangeable protons from both the water and sugar hydroxyl groups around the single labeled nonexchangeable H4 atom is

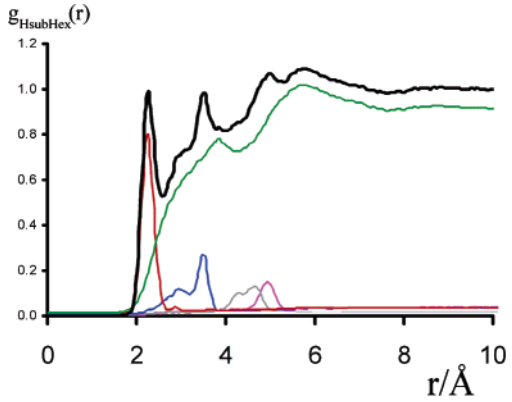

Figure 4. The function $g_{H_{sub}H_{ex}}(r)$ as calculated from MD, top black line. The subcomponents of this function due to the different types of exchangeable hydroxyl protons H_{ex} are also shown; the contributions for H_{ex} on water (green line), HO4 (red), HO3 (blue), HO2 (gray), and HO1 (purple) are illustrated.

displayed in Figure 4. This function may be viewed as having two components: correlations to $H_{ex}X$, which include several very strong intramolecular components due to hydroxyl hydrogen atoms on the same molecule, and intermolecular correlations to water, exhibiting structure out to about 8 Å. The calculated individual intramolecular contributions to $g_{H_{sub}H_{ex}}(r)$ from each hydroxyl group in the xylose molecule are also shown in Figure 4. Several features of the total $g_{H_{sub}H_{ex}}(r)$ function can easily be ascribed to specific hydroxyl groups of the xylose. Specifically, the peak at 2.2 Å is due to the hydroxyl group on the C4 carbon, the peak at 3.5 Å to that on C3, and the peak at 5 Å to those on C2 and C1 combined. While the first peak due to the C4 hydroxyl group is a singlet, the C3 and C2 components actually consist of doublets due to the two distinct distances arising from the different conformational minima of these hydroxyl groups. The lower-*r* sub-peak of the C3 component contributes to the total $g_{H_{sub}H_{ex}}(r)$ as a shoulder to the second peak around 2.8−2.9 Å.

Much of the structure in the intermolecular component of $g_{H_{sub}H_{ex}}(r)$ is due to the exclusion of water molecules by the presence of the other atoms of the sugar solute. However, this intermolecular component exhibits a clear, broad peak just below 4 Å due to the water molecules hydrating this hydrophobic group and to those hydrogen bonded to the adjacent hydroxyl group, but as can be seen in Figure 4, this peak barely registers in the cumulative function, and its position actually corresponds to a broad minimum on this total function due to the sharper decay in the correlation with the HO3 atom. Such entanglement greatly complicates any effort to extract direct information about the hydration of the C4 group from the experimental data, which cannot be resolved into components.

Figure 5 compares the calculated and experimental structure factors for the exchangeable protons about the labeled H4, and Figure 6 compares the radial distribution functions calculated from these structure factors. Unlike the case for the total atomic radial distribution function ${}^{H_2O}G^{Y}_{H_{sub}}(r)$ (Figure 2b), the agreement between the MD simulations and the experiment for the exchangeable hydrogen contribution $g_{H_{sub}H_{ex}}(r)$ is less satisfactory (Figure 6). Although the *Q*-range of the D20 diffractometer is nominally 0.9−13 $Å^{-1}$, for this double-difference experiment the data are probably only statistically reliable for the range 0.9−5.0 $Å^{-1}$, based on the signal-to-noise ratio, since the signal beyond 5.0 $Å^{-1}$ is very small while the noise remains comparable. The lack of reliable *Q*-range means that the *r*-space molecular correlations are severely resolution-limited. While the first-order difference method requires measurements for only two solutions, and can be accurately performed at contrast levels of a few millibarns,[38] the method for the determination of $g_{H_{sub}H_{ex}}(r)$ requires four solutions to be measured, and consequentially counting statistics are a much greater source of error. Due to the limited availability of beam time, it is not practical to gather data on a sample for more than about 8 h. It would therefore not have been practical to greatly enhance the counting statistics for these data, as acquisition was performed on the D_2O solutions for 4 h and on the H_2O solutions for 8 h (due to the much higher level of incoherent scattering from these ^1H-rich samples). As a result, the Fourier transform of $S_{H_{sub}H_{ex}}(Q)$ yields significant errors due to the poor signal-to-noise ratio in the region 5−13 $Å^{-1}$. Further, it was found that if the $g_{H_{sub}H_{ex}}(r)$ calculated from MD was back-transformed and retransformed using only the region 0−5 $Å^{-1}$ (applying the resolution of the reliable portion of the data to the MD $g_{H_{sub}H_{ex}}(r)$), the imposed resolution broadens the modeling data significantly (Figure 6).

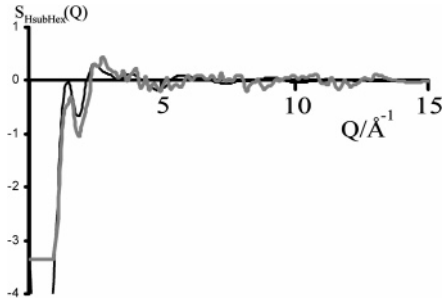

Figure 5. $S_{H_{sub}H_{ex}}(Q)$ as calculated from MD simulation (black) and measured by neutron scattering (gray). Unlike in Figure 3, the *Q*-range does not limit the resolution of the measurement here; however, the lack of low-*Q* data does.

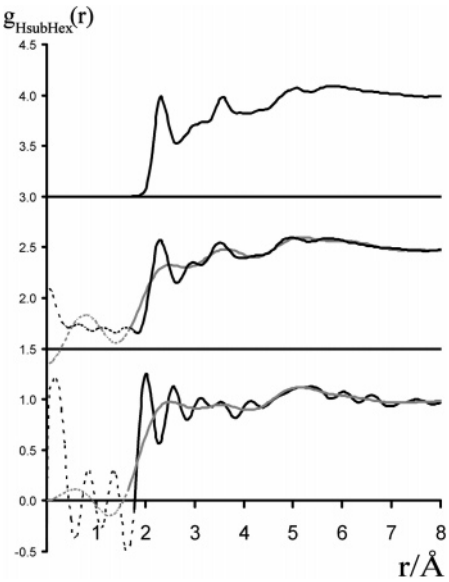

Figure 6. The function $g_{H_{sub}H_{ex}}(r)$ as calculated from the MD simulation, upper black line. The lower and middle black lines are the experimental and MD $g_{H_{sub}H_{ex}}(r)$ functions, respectively, in each case with the full experimental resolution applied (0.9−13 $Å^{-1}$). The lower and middle gray lines show the experimental and MD function $g_{H_{sub}H_{ex}}(r)$, respectively, in each case from the *Q*-range for which the experimental data are statistically reliable (0.9−5.0 $Å^{-1}$). In all cases the unphysical ringing below about 1.7 $Å^{-1}$ is shown by a broken line.

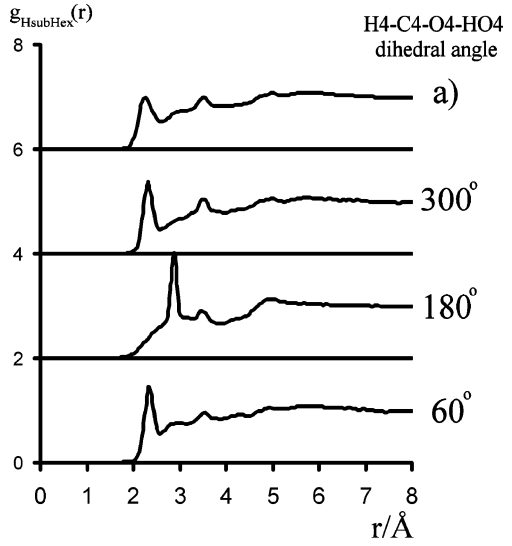

Figure 7. Radial distribution function $g_{H_{sub}H_{ex}}(r)$ as calculated from the MD simulations: a, as calculated from the unconstrained simulation; 300°, 180°, and 60°, as calculated from the simulations with the H4−C4−O4−HO4 torsional angle constrained to each of the specified angles.

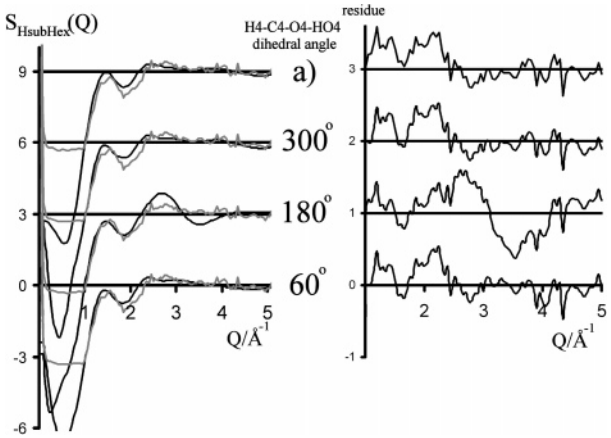

Figure 8. Structure factor $S_{H_{sub}H_{ex}}(Q)$ as calculated from the MD simulations and determined from NDIS experiments. Left: a, $S_{H_{sub}H_{ex}}(Q)$ as calculated from the unconstrained simulation; 300°, 180°, and 60°, $S_{H_{sub}H_{ex}}(Q)$ as calculated from the simulations with the H4−C4−O4−HO4 torsional angle constrained to each of the specified values. In each case the experimental NDIS data is overlain in gray. Right: the residue from subtracting the NDIS data from the MD simulation curve. The 180° case gives a particularly poor fit over the reliable portion of the NDIS data.

In principle, from $g_{H_{sub}H_{ex}}(r)$ it should be possible to describe the intramolecular correlations between the labeled H4 atom and the hydroxyl hydrogen atoms experimentally, which could be used to extract the rotameric conformational distribution of the O4 hydroxyl group, since the H4−HO4 distance changes as this group rotates about the C4−O4 bond (Figure 7; also see Figure 1). To examine the sensitivity of the function $S_{H_{sub}H_{ex}}(Q)$ to the O4−HO4 dihedral angle, this function was calculated from simulations with the H4−C4−O4−HO4 dihedral constrained to angles of 60°, 180°, and 300° (Figure 8). It was found that this function varied significantly with angle in the region 0−5 Å^{-1}; in particular the 180° position was unique in having a significant maximum and minimum at 2.7 Å^{-1} and 3.5 Å^{-1}, respectively. Furthermore, all three conformations gave different reciprocal space representations at $Q < 1$ Å^{-1}. Although it is possible to measure such a Q-range with two-axis diffractometers such as D20, this would entail a different instrument setup

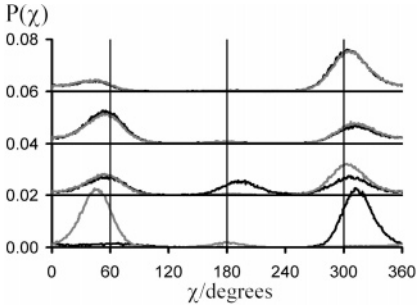

Figure 9. Rotameric population probability distributions for each of the four hydroxyl groups in D-xylopyranose as calculated from the MD simulation, in increasing carbon number from the bottom. A value of χ of 180° corresponds to a geometry trans to H4, while 60° corresponds to gauche-plus and 300° corresponds to gauche-minus. Note the highly uneven distribution of rotamers, with some significantly preferred. For each carbon, the black line is the data calculated from the α-D-xylopyranose simulation and the gray line is for the β anomer.

that would preclude measurement of the higher Q-range. Although the statistical errors in the neutron scattering data are consistent across the entire Q-range, the model predicts a large signal in $S(Q)$ in the region 0−5 Å^{-1}. From comparison of the MD and experimental $S(Q)$ data for $S_{H_{sub}H_{ex}}(Q)$, it is clear that there is considerable statistical noise in these data, yielding a standard deviation of 1.2 mb str^{-1} atom^{-1} for data re-binned in Q-steps of 0.5 Å^{-1}. The comparison is therefore performed in the region 0−5 Å^{-1}, where there is a relatively high signal-to-noise ratio compared to the rest of $S_{H_{sub}H_{ex}}(Q)$. Of the three principal expected energetic minima at 60°, 180°, and 300°, it was found that the 180° position gave a significantly poorer fit to the experimental data than the other two positions and could be reasonably precluded by this physical measurement. This result was quantified by the summation of the absolute difference between the experimental and MD-calculated function for each position in the region 1−5 Å^{-1}. For the 60°, 180°, 300°, and unconstrained simulations this yielded values of 12, 21, 13, and 14 mb str^{-1} atom^{-1}, respectively.

While a significantly lower-noise measurement over a wider Q-range might allow the 60° and 300° positions to be distinguished, it was found that with the data presented here this was not possible, nor was it possible to distinguish between the functions calculated from the 60° and 300° constrained simulations and the unconstrained function. The MD simulations suggest that the rotational conformation of the HO4−O4 hydroxyl group is insensitive to the anomeric conformation of the sugar, in both cases showing populations of about 75% for the 300° conformer and 25% for the 60° positions, with the 180° position essentially unoccupied (Figure 9). The 300° conformer is preferred because it optimizes electrostatic interactions with the O3 oxygen atom without precluding hydrogen bonds to water, but it is not clear why the 180° conformer, which would allow the geometrically most optimal hydrogen-bonding to water, would be so disfavored. It appears that this preference arises entirely from intramolecular interactions, since in the trans conformer at 180° this hydroxyl proton is approximately 2.5 Å away from two like-charged aliphatic protons on C5 and C3 (see Figure 1), while in the gauche positions there is only one such repulsive interaction at ∼2.5 Å, with the C4 proton. This distribution differs from that observed previously[39] using an

(39) Schmidt, R. K. Ph.D. Thesis, Cornell University, Ithaca, NY, 1995.

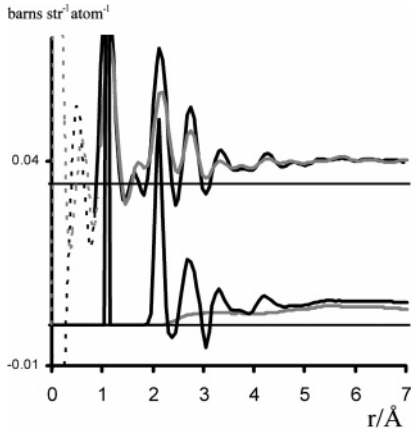

Figure 10. MD simulation of the best experimental function that can be measured by NDIS by H/D substitution at the H4 position. The constitution of this measurement is $3.92g_{H_{sub}Ow}(r) + 1.05g_{H_{sub}Og}(r) + 1.21g_{H_{sub}C}(r) - 0.68g_{H_{sub}H_{non}}(r)$ (lower black line); the $g_{H_{sub}Ow}(r)$ component is shown at the bottom in gray. Although the correlation from the substituted nucleus to the hydrating water is the dominant term, the signal in the crucial region up to about 6 Å is dwarfed by intramolecular correlations. At the top is shown the function as measured by NDIS (gray) and the MD simulation after it has had the experimental limits imposed upon it.

earlier version of the CHARMM parameters for sugars.[25] However, the present results demonstrate that it is possible to distinguish between these positions, due to their different three-dimensional structure.

The goal of this study was to probe the water oxygen density around the D-xylose sugar molecule. However, since the solvent is most strongly ordered in response to the hydroxyl groups and not to the sites that can be individually examined (the nonexchangeable hydrogen atoms), it follows that the interpretation of the experimental results is difficult. The situation is further complicated by the intramolecular correlations of the xylose molecule itself, which cannot be simply removed and are considerably more structured than the correlations of the substituted hydrogen to the water molecules. This problem is emphasized in Figure 10, where the MD simulation of the best structural measurement that can be made is shown. Despite the fact that correlations between the hydrating water and the xylose contribute over 60% of this measurement (with a $g_{H_{sub}Ow}(r)$ prefactor of 3.92 mb), in the crucial region up to about 5 Å this contribution is dwarfed by the intramolecular correlations. Currently the differences between the MD simulation and the NDIS measurement of the molecule, while relatively minor in themselves, are large compared to the expected signal from those water molecules hydrating the xylose. In order for further progress to be made, a new approach will be required that is capable of accurately removing the intramolecular structure from NDIS measurement.

Conclusions

The studies reported here represent the first attempt to use NDIS experiments to characterize specific atomic details about the structure of sugar solutions. The experiment reported here was intended to collect data about correlations between the substituted hydrogen and, first, the H_{ex} atoms and second, the C, O, and H_{non} atoms. To get the function $G^{Y}_{H_{sub}}(r)$, it was necessary to combine four neutron scattering measurements. However, it is possible to obtain only the function $G^{Y}_{H_{sub}}(r)$ by neutron scattering measurements on only two solutions (the H/D-substituted xylose in a solution in which the H_{ex} atom has an average coherent scattering length of 0). This experiment would require less beam time and would provide significantly better counting error per hour of beam time; however, it would not provide as much information as the method employed here.

The present results allowed the conformation of the hydroxyl group on the same carbon atom as the isotopically substituted hydrogen atom H4 to be estimated, thus providing a test for the modeling. A major goal of these studies was to determine the nature of water structuring around the solute. For complex asymmetric solutes such as sugars, this effort is complicated by the fact that each nonexchangeable proton in the system is in a different environment, which is why the present study employed xylose solutes specifically labeled only at one position, on the C4 carbon, which in principle allows the extraction of the structure of exchangeable protons around just this atom. Even in this case, however, in addition to the desired solvent contribution, the experimental $g_{H_{sub}H_{ex}}(r)$ also contains large intramolecular contributions from the exchangeable hydroxyl hydrogen atoms which obscure the solvent contribution. As was seen, this intramolecular contribution makes a purely experimental measurement of just the solvent contribution impossible from the present data alone.

Several alternate approaches might be attempted to separate out the hydration contribution in future studies. For example, a hybrid approach might be possible where the intramolecular contribution could be evaluated from the MD simulations, if they were sufficiently reliable, and then subtracted out from the experimental function to give the residual contribution from solvent only. This "experimental" solvent structuring could then be compared to that calculated solely from the modeling. The principal problem with this approach is that, at present, the modeling methodology is not of sufficient quality to make this approach definitive. However, due to the relatively constrained nature of the sugar structure, it should be possible to improve the quality of the molecular mechanics energy functions so as to reproduce the experimental observation.

A principal result of the present study was the determination that the O4 hydroxyl group avoids the trans conformation at 180°, apparently due principally to intramolecular interactions. The MD simulation results further indicate that the 300° gauche conformation is preferred due to favorable intramolecular electrostatic interactions, although the O4−HO4−O3 angle is too strained for this interaction to be considered a proper hydrogen bond. Such a result might be expected for this sugar in a vacuum, but it is less obvious for the solvated molecule and demonstrates that, at least for this functional group, the solvent structuring is probably dictated by the intramolecular conformational structure rather than the other way around. It is possible that such intramolecular energetic considerations might also govern the interactions of sugar molecules with other molecules, such as in binding to proteins.

Acknowledgment. The authors gratefully acknowledge the assistance of G. Cuello and T. Hansen of the ILL. This project was supported by grant GM63018 from the National Institutes of Health.

JA051376L